Journal of Asian Earth Sciences 94 (2014) 1–11

Contents lists available at ScienceDirect

Journal of Asian Earth Sciences

journal homepage: www.elsevier.com/locate/jseaes

Anticlockwise P-T evolution at ~280 Ma recorded from ultrahigh-temperature metapelitic granulite in the Chinese Altai orogenic belt, a possible link with the Tarim mantle plume?

Laixi Tong [a,*], Yi-Gang Xu [a], Peter A. Cawood [b], Xin Zhou [a,c], Yibing Chen [a], Zhao Liu [a,c]

[a] State Key Laboratory of Isotope Geochemistry, Guangzhou Institute of Geochemistry, Chinese Academy of Sciences, Guangzhou 510640, China
[b] Department of Earth Sciences, University of St Andrews, Fife KY16 9AL, Scotland, UK
[c] University of Chinese Academy of Sciences, Beijing 10049, China

ARTICLE INFO

Article history:
Received 28 January 2014
Received in revised form 29 July 2014
Accepted 30 July 2014
Available online 10 August 2014

Keywords:
Ultrahigh-temperature metamorphism
The Chinese Altai
P-T path
U–Pb age
Mantle plume

ABSTRACT

An ultrahigh-temperature (UHT) metapelitic granulite assemblage consisting of garnet(g)–spinel(sp)–orthopyroxene(opx)–sillimanite(sil)–cordierite(cd)–ilmenite(ilm)–biotite(bi)–plagioclase(pl)–quartz(q) occurs within migmatitic paragneiss near Kalasu in the Chinese Altai, NW China. Textural relations, mineral compositions and P-T estimates, indicate three stages of mineral assemblages: (1) pre-peak prograde stage (M1) consisting of a sp–sil-bearing or sp–opx-bearing inclusion assemblage, with low-Al_2O_3 contents (4–5 wt.%) in orthopyroxene and P-T conditions of ~7 kbar and ~890 °C, (2) peak UHT stage (M2) comprising a g–opx–cd-bearing coarse-grained assemblage, with high-Al_2O_3 contents (8–9 wt.%) in orthopyroxene and peak conditions of ~8 kbar and ~970 °C, and (3) post-peak HT stage (M3) containing an oriented opx–bi–sil-bearing assemblage in matrix, with moderate amounts of Al_2O_3 (6–7 wt.%) in orthopyroxene and P-T conditions of 8–9 kbar and ~870 °C. The three discrete stages define an anticlockwise P-T path involving initial prograde heating and post-peak near isobaric cooling. Such a near isobaric cooling anticlockwise P-T path suggests that UHT metamorphism likely occurred in an overall extensional tectonic setting with associated underplating of mantle-derived mafic magma. A SHRIMP zircon U–Pb age of 278 ± 2 Ma obtained from the metapelitic granulite indicates UHT metamorphism in the Altai orogen occurred during the Permian, coeval with spacially associated mantle-derived mafic intrusions (~280 Ma) and the Tarim mantle plume (~275 Ma). Thus, the Permian UHT metamorphism of the Chinese Altai is likely associated with underplating and heating of mantle-derived mafic magma as a result of the Tarim mantle plume.

1. Introduction

The study of ultrahigh-temperature (UHT) metamorphism can provide important insight into the formation and evolution of deep continental crust (Harley, 2004). UHT metamorphism involves very high temperature granulite-facies conditions in which crustal rocks experienced peak temperature in excess of 900 °C, and is generally characterized by mineral assemblages such as opx + sil + q, sa + q, crn + q, sp + q, and osm + g (opx, orthopyroxene; sil, sillimanite; q, quartz; sa, sapphirine; crn, corundum; sp, spinel; osm, osumilite; and g, garnet), while the orthopyroxene contains over 8.0 wt.% Al_2O_3 (Harley, 2004, 2008). The pressure range is mainly located in the sillimanite stability field (Brown, 2007). Some 30 localities of UHT granulites have been reported worldwide; most are restricted to Precambrian high-grade metamorphic terranes (Brown, 2007), including those in East Antarctica, South India and North China (Raith et al., 1997; Harley and Motoyoshi, 2000; Tong and Wilson, 2006; Santosh et al., 2007). As UHT granulites contain important information on the processes of lower crust evolution and possible crust-mantle interaction, the study of these rocks is scientifically critical to understanding tectonothermal evolution of the lithosphere.

In the last several years, mafic and metapelitic granulites have been reported from the Chinese Altai orogenic belt (Li et al., 2004; Chen et al., 2006a, 2006b; Wang et al., 2009). Furthermore, Li et al. (2010) reported an occurrence of a UHT (>900 °C) metapelitic granulite at Wuqiagou in Fuyun county. The P-T path of the UHT metapelitic granulite and the timing of the UHT metamorphism are not yet resolved. Li et al. (2010) dated the UHT metamorphism at ~499 Ma, whereas Li et al. (2012) gave its age as

* Corresponding author. Tel.: +86 20 38383127; fax: +86 20 85290130.
E-mail address: lxtong@gig.ac.cn (L. Tong).

http://dx.doi.org/10.1016/j.jseaes.2014.07.043
1367-9120/

~277 Ma. In this paper we outline the petrography, P-T estimates and chronology of a garnet–orthopyroxene–sillimanite–cordierite-bearing UHT granulite, documenting an anticlockwise P-T evolution path and proposing that a synchronous mantle plume was responsible for the UHT metamorphism.

2. Geological background

The Altai orogenic belt constitutes part of the Central Asian Orogenic Belt, a Neoproterozoic to late Palaeozoic accretionary orogen (Sengör et al., 1993; Jahn, 2004; Jahn et al., 2004; Xiao et al., 2004, 2010; Cawood et al., 2009). The Altai orogenic belt is situated on the south-western margin of the Siberian plate, and its southern boundary with the Junggar plate is delineated by the large NW-trending Erqis fault (Fig. 1) (He et al., 1990; Windley et al., 2002). The belt is divided into five fault-bounded terranes or tectonic units (He et al., 1990; Windley et al., 2002; Xiao et al., 2004; Wang et al., 2006, 2009). Unit I and Unit II are composed of the Devonian–Carboniferous volcanic-sedimentary rocks and Neoproterozoic–Ordovician and minor Devonian sedimentary–volcanic rocks, respectively, and mostly underwent greenschist facies metamorphism. Unit III (or the central Altai terrane) consists largely of Neoproterozoic–Ordovician metasedimentary and metavolcanic rocks, and constitutes a micro-continent block. The rocks in this unit generally experienced greenschist to amphibolite facies metamorphism. Unit IV (or the Qiongkuer–Abagong terrane) contains late Silurian to early Devonian arc-type volcanic and pyroclastic rocks, displaying greenschist to upper amphibolite facies metamorphism and locally granulite facies conditions (Chen et al., 2006a; Wang et al., 2009; Li et al., 2010). Unit V (or the Erqis terrane) is composed of Precambrian basement and Devonian–Carboniferous volcaniclastic rocks, metamorphosed at greenschist to amphibolite facies conditions.

About 40% of the Altai orogenic belt is composed of granitoids and orthogneiss consisting mainly of early Palaeozoic syn-orogenic and late Palaeozoic post-orogenic and anorogenic granitic bodies, which may be subdivided into tonalite, granodiorite and biotite granite, with minor two mica granite (Wang et al., 2006). The ages of the former are mainly around ~400 Ma (ranging from 450 to 370 Ma), and show a magmatic arc geochemical signature (Wang et al., 2006; Yuan et al., 2007; Sun et al., 2008), whereas the ages of the latter are mostly between 280 and 270 Ma (Wang et al., 2005; Tong et al., 2006a; Zhou et al., 2007; Zhang et al., 2010, 2012), and a mantle-derived geochemical signature (Tong et al., 2006b). Additionally, there are also some mantle-derived mafic intrusive rocks and an ultramafic intrusive complex dated at about 280 Ma at Kalatongke and Wuqiagou in Fuyun county (Han et al., 2004; Chen and Han, 2006). These Permian ages are similar to the timing of movement on the Erqis shear zone (Laurent-Charvet et al., 2003; Briggs et al., 2007).

The Chinese Altai orogenic belt displays extensive development of Palaeozoic medium–low-pressure grade metamorphic zones and several granitic-gneissic thermal dome structures (Zhuang, 1994; Zhang et al., 2004; Xu et al., 2005; Wei et al., 2007). The metamorphic zones can be divided into kyanite-type and andalusite-type, and Windley et al. (2002) thought that the belt had features characteristic of a Barrovian-type metamorphic zone. The high-temperature portion in the andalusite-type zone develops a garnet-cordierite zone (Fig. 1) (Zhuang, 1994; Wei et al., 2007), which reached granulite facies metamorphic conditions (Wang et al., 2009). Zhuang (1994) reported an Rb–Sr whole-rock isochron of 365 Ma and Hu et al. (2002) a U–Pb zircon lower intercept age of

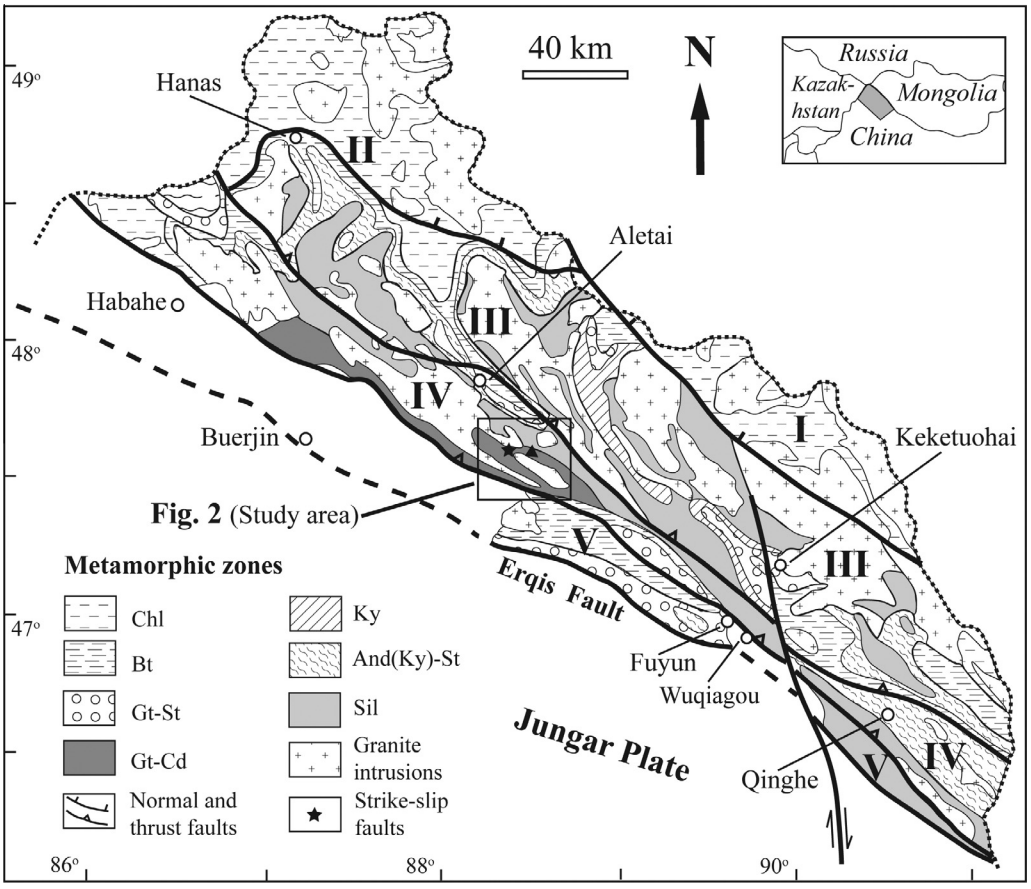

Fig. 1. Metamorphic map of the Chinese Altai orogen (modified after Wei et al., 2007).

367 Ma from the gneisses in the region. These Devonian ages were interpreted to represent the time of the major greenschist–amphibolite facies metamorphism (Windley et al., 2002; Wei et al., 2007). More recently, zircon U–Pb age data further support early amphibolite facies metamorphism at 390–380 Ma (Long et al., 2007; Zheng et al., 2007; Jiang et al., 2010). This has led to two different opinions on the evolution history of the region: Devonian arc-continent collision (Windley et al., 2002; Wang et al., 2006; Wei et al., 2007), or a ridge-subduction and slab-window model accompanied by low-pressure high-temperature metamorphism (Windley et al., 2007; Sun et al., 2009; Jiang et al., 2010).

Additional zircon U–Pb and monazite Th–Pb ages of 290–260 Ma have been reported from the granulites or gneisses in the region (Hu et al., 2006; Chen et al., 2006b; Briggs et al., 2007; Zheng et al., 2007; Wang et al., 2009), indicating that the Altai orogenic belt experienced a significant high-grade structural metamorphic event in the late Palaeozoic (Xiao et al., 2006, 2008). For instance, Wang et al. (2009) recognized medium–low-pressure high-temperature (HT) (~800 °C) metapelitic granulites near Dakalasu of Aletai, and Li et al. (2010) reported a UHT (>900 °C) metapelitic granulite assemblage from Wuqiagou of Fuyun county, and conflicting ages of ~499 Ma and 270–290 Ma were obtained from the UHT metapelitic granulite (Li et al., 2010, 2012). A number of different interpretations have been placed on the origin of the Permian high-grade metamorphic event; for instance, the Altai orogeny was subjected to an oceanic subduction and plate collision in the Permian that was responsible for the high-temperature or UHT granulite metamorphism (Chen et al., 2006a; Li et al., 2012), the Permian granulite facies metamorphism occurred in an extensional tectonic setting (Wang et al., 2009), or the Altai orogeny was associated with a Permian mantle plume event (Pirajno et al., 2008; Zhang et al., 2010; 2012).

The UHT metapelitic granulite sample (LT10F) presented in this study was collected near Kalasu village, southeast of Aletai city (47°35′38″N, 88°20′18″E), occurring as rare tectonic lenses within the medium–low-pressure garnet–cordierite–sillimanite-bearing metapelitic granulite zone reported by Wang et al. (2009) (Fig. 2). Moreover, this metapelitic granulite zone shows a feature of ductile shear deformation and contains small amounts of garnet-bearing calcsilicate granulites, post-tectonic pegmatite veins, and Permian mafic intrusions (Zhang et al., 2012). The UHT metapelitic granulites and medium–low-pressure metapelitic granulites developed banded structures and generally experienced partial melting and migmatitization, the latter displaying D1 folding and D2 shear fabrics.

3. Petrography and mineral chemistry

Minerals in the UHT metapelitic granulite (Table 1) were analysed with a JXA-8100 microprobe at State Key Laboratory of Isotopic Geochemistry, Guangzhou Institute of Geochemistry, Chinese Academy of Sciences, with an accelerating voltage of 15 kV, a beam current of 3×10^{-8} Å, a beam width of 1 μm, and data correction by using a ZAF method. Representative mineral compositions for the studied sample are listed in Table 1.

The UHT metapelitic granulite (LT10F) contains garnet (10%), orthopyroxene (7–8%), cordierite (10–12%), sillimanite (2–3%), spinel (4–5%), biotite (15–20%), plagioclase (15–20%), quartz (20–25%), and minor ilmenite and magnetite. No K-feldspar was observed in the assemblages, which are similar to the mineral assemblages in the UHT metapelitic granulite at Wuqiagou reported by Li et al. (2010). The petrographic observations show that the rock develops at least two fabrics, S1 and S2 (Fig. 3a), probably in response to two episodes of deformation D1 and D2. The S1 fabric consists mainly of coarse-grained less deformed garnet–orthopyroxene–biotite-bearing mineral assemblage, whereas the S2 fabric is composed of a mineral assemblage of biotite–orthopyroxene–sillimanite–plagioclase–quartz showing marked preferred orientation (Fig. 3a and f). Coarse-grained cordierite grains contain

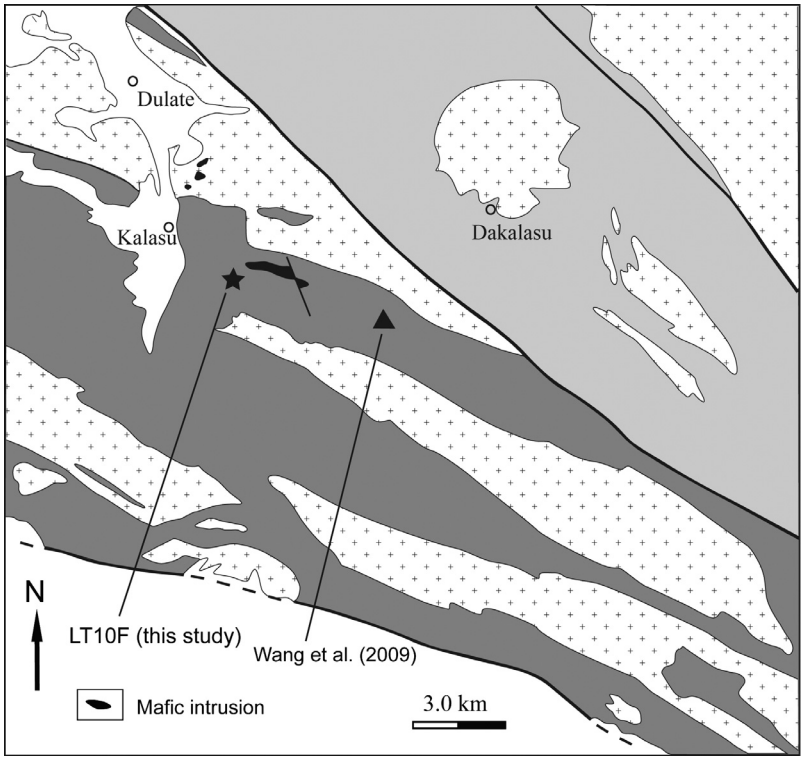

Fig. 2. Metamorphic map of the study area, showing the sample location, and symbols are same as those of Fig. 1.

Table 1
The EPMA analysis results of representative minerals in the UHT metapelitic granulite (wt.%), in which Fe_2O_3 and FeO contents are recalculated assuming stoichiometry. Abbreviations: g(c), garnet core; g(m), middle garnet between core and rim; g(r), garnet rim; opx(i), orthopyroxene inclusion in garnet; opx(c), orthopyroxene core; opx(m), middle orthopyroxene between core and rim; opx(r), orthopyroxene rim; opx(2), M2 orthopyroxene; ilm(i), ilmenite inclusion; sp(i), spinel inclusion; sp(o), spinel in matrix; mt(e), magnetite needle in orthopyroxene; cd(i), cordierite inclusion; bi(i), biotite inclusion; bi(c), biotite core; and bi(r), biotite rim. X_{Mg} = Mg/(Fe^{2+} + Mg); X_{Al} = Al/2.

	g(c)	g(m)	g(r)	opx(i)	opx(c)	opx(m)	opx(r)	opx(3)	sil	ilm(i)	sp(i)	sp(o)	mt(e)	cd(i)	cd	bi(i)	bi(c)	bi(r)	pl	pl
SiO_2	38.88	37.92	39.06	50.51	46.70	47.25	48.23	47.87	37.62	1.67	0.03	0.02	0.12	50.69	49.71	37.36	36.22	35.92	60.85	56.26
TiO_2	0.07	0.06	0.06	0.09	0.06	0.08	0.04	0.05	0.02	39.71	0.04	0.00	0.11	0.00	0.06	4.72	4.57	3.81	0.01	0.00
Al_2O_3	22.02	22.25	21.6	5.13	8.95	8.18	6.29	6.84	60.94	0.57	59.14	57.44	0.18	33.20	33.96	16.89	16.60	16.27	24.35	27.09
Cr_2O_3	0.03	0.01	0.03	0.00	0.00	0.00	0.00	0.01	0.04	0.05	0.25	1.16	2.16	0.00	0.00	0.09	0.12	0.09	0.00	0.02
Fe_2O_3	0.00	1.20	0.00	0.00	2.56	3.07	2.37	1.80	0.88	23.30	5.47	4.74	63.51	0.13	0.94	0.00	0.00	0.00	0.03	0.06
FeO	28.48	27.63	30.20	23.52	22.23	22.56	22.61	23.70	0.00	34.92	23.50	27.60	29.93	3.91	3.40	10.89	14.31	14.89	0.00	0.00
MnO	1.10	0.95	1.17	0.21	0.29	0.19	0.23	0.54	0.00	0.73	0.09	0.07	0.09	0.02	0.05	0.03	0.01	0.00	0.00	0.02
MgO	8.44	8.62	6.68	20.51	18.66	18.92	19.54	18.45	0.01	1.12	10.42	6.58	0.05	11.24	11.21	15.88	13.77	13.77	0.01	0.00
CaO	1.24	1.05	1.42	0.05	0.03	0.04	0.03	0.05	0.08	0.00	0.00	0.00	0.00	0.01	0.01	0.04	0.00	0.00	5.72	9.69
Na_2O	0.00	0.02	0.01	0.00	0.01	0.01	0.00	0.02	0.00	0.01	0.08	0.14	0.00	0.14	0.09	0.60	0.22	0.22	8.74	6.20
K_2O	0.00	0.00	0.00	0.00	0.01	0.00	0.00	0.00	0.00	0.00	0.00	0.01	0.00	0.01	0.00	9.81	10.14	10.84	0.16	0.09
ZnO											1.39	2.32								
Totals	100.3	99.59	100.23	100	99.25	100.00	99.11	99.15	99.59	99.75	99.86	99.60	96.15	99.34	99.43	96.32	95.96	95.82	99.85	99.41
O	12	12	12	6	6	6	6	6	10	3	4	4	4	18	18	11	11	11	8	8
Si	3.000	2.944	3.040	1.886	1.763	1.774	1.825	1.820	2.043	0.041	0.001	0.001	0.004	5.057	4.962	2.713	2.692	2.696	2.711	2.543
Ti	0.004	0.004	0.004	0.003	0.002	0.002	0.001	0.001	0.001	0.735	0.001	0.000	0.003	0.000	0.005	0.258	0.255	0.215	0.000	0.000
Al	2.003	2.037	1.982	0.226	0.398	0.362	0.281	0.307	3.901	0.017	1.890	1.895	0.008	3.905	3.997	1.446	1.455	1.440	1.279	1.444
Cr	0.002	0.001	0.002	0.000	0.000	0.000	0.000	0.000	0.001	0.001	0.005	0.026	0.064	0.000	0.000	0.005	0.007	0.005	0.000	0.001
Fe^{3+}	0.000	0.070	0.000	0.000	0.073	0.087	0.068	0.051	0.036	0.431	0.106	0.086	1.913	0.010	0.071	0.000	0.000	0.000	0.001	0.002
Fe^{2+}	1.838	1.795	1.966	0.734	0.702	0.708	0.716	0.754	0.000	0.719	0.542	0.660	1.002	0.326	0.284	0.661	0.890	0.935	0.000	0.000
Mn	0.072	0.062	0.077	0.007	0.009	0.006	0.007	0.017	0.000	0.015	0.002	0.002	0.003	0.002	0.004	0.002	0.001	0.000	0.000	0.001
Mg	0.971	0.998	0.775	1.141	1.050	1.058	1.102	1.045	0.001	0.041	0.421	0.275	0.003	1.671	1.668	1.719	1.525	1.540	0.001	0.000
Ca	0.103	0.087	0.118	0.002	0.001	0.002	0.001	0.002	0.005	0.000	0.000	0.000	0.000	0.001	0.001	0.003	0.000	0.000	0.273	0.469
Na	0.000	0.003	0.002	0.000	0.001	0.001	0.000	0.001	0.000	0.001	0.004	0.008	0.000	0.027	0.017	0.084	0.032	0.032	0.755	0.543
K	0.000	0.000	0.000	0.000	0.000	0.000	0.000	0.000	0.000	0.000	0.000	0.000	0.000	0.001	0.000	0.909	0.962	1.038	0.009	0.005
Zn											0.028	0.048								
Sum	7.993	8	7.965	3.999	4	4	4	4	5.988	2	3	3	3	11	11.008	7.801	7.819	7.902	5.030	5.008
X_{Mg}	0.346	0.357	0.283	0.609	0.599	0.599	0.606	0.581			0.437	0.294		0.837	0.855	0.722	0.631	0.622		
X_{Al}				0.113	0.199	0.181	0.141	0.154												

spinel and sillimanite inclusions (Fig. 3b), whereas garnet porphyroblast also contains spinel and orthopyroxene inclusions (Fig. 3c). These textural relations suggest that the early M1 assemblage comprises spinel–sillimanite-bearing and spinel–orthopyroxene-bearing inclusion assemblages. Peak M2 mineral assemblage is indicated by the coarse-grained less deformed assemblage garnet–orthopyroxene–biotite–cordierite–plagioclase–quartz associated with development of the S1 fabric (Fig. 3c and e). The orthopyroxene and spinel inclusions in the garnet display retrograde biotite and cordierite, respectively (Fig. 3c), while some oriented fine magnetite needles are also observed in the orthopyroxene grains (Fig. 3d). The M3 mineral association is indicated by the assemblage of orthopyroxene–biotite–sillimanite–plagioclase ± cordierite–magnetite–quartz showing marked preferred orientation in the matrix (Fig. 3f).

Garnet compositions show an overall decrease in MgO content and a slight increase in CaO content from core to rim (Fig. 4). In detail MgO content shows a slight increase (8.6 wt.%) and then decrease from the core (8.4 wt.%) to the rim (6.7 wt.%), with the corresponding X_{Mg} (=Mg/(Fe^{2+} + Mg)) values of 0.346, 0.357 and 0.283, respectively. An orthopyroxene inclusion has an X_{Mg} value of 0.609 and contains a low Al_2O_3 content (5.1 wt.%) (as low as 4.5 wt.%), with a corresponding X_{Al} (=Al/2) value of 0.113 in the formula. Peak M2 orthopyroxene has markedly higher Al_2O_3 contents than those of the M1 orthopyroxene inclusion and M3 orthopyroxene, and the core shows a highest Al_2O_3 content of 8.95 wt.%, remarkably higher than that of its rim (6.3 wt.%), with the corresponding X_{Al} values of 0.199 and 0.141. Cordierite is rich in MgO, with the X_{Mg} values of 0.855 and 0.837. Spinel inclusions have a lower ZnO content (1.4 wt.%) than that of matrix spinel (2.3 wt.%), with the corresponding X_{Mg} values of 0.437 and 0.294, respectively. Sillimanite contains an Fe_2O_3 content of 0.88 wt.%. Biotite shows a decrease in TiO_2 content from the core (4.6 wt.%) to the rim (3.8 wt.%), with resultant X_{Mg} values of 0.631 and 0.622, respectively. Anorthite contents in plagioclase range from An_{31} to An_{46}.

In summary, that Al_2O_3 content exceeds 8.0 wt.% in peak orthopyroxene indicates that peak metamorphism in the metapelitic granulite reached UHT conditions (>900 °C) (Harley, 2004). Moreover, the textural relations and mineral compositions show that three-stage mineral assemblages can be distinguished: (1) pre-peak spinel–orthopyroxene-bearing or spinel–sillimanite-bearing inclusion assemblage (M1), characterized by low Al_2O_3 contents (4–5 wt.%) in orthopyroxene; (2) peak garnet–orthopyroxene–cordierite–K-feldspar-bearing UHT mineral assemblage (M2), characterized by high Al_2O_3 contents (8–9 wt.%) in orthopyroxene; and (3) post-peak orthopyroxene–sillimanite–biotite–magnetite-bearing HT mineral assemblage (M3), with a feature of medium Al_2O_3 contents (6–7 wt.%) in orthopyroxene.

4. P-T estimates and P-T path

Equilibrated mineral pairs or mineral assemblages can be used to estimate the metamorphic P-T conditions in the UHT metapelitic granulite, but many traditional garnet–orthopyroxene thermobarometers fail to consider the effects of Fe^{2+}–Mg reset that can occur between mineral pairs during the cooling after peak HT granulite facies metamorphism, and cannot give true peak or pre-peak P-T conditions. Therefore, in this paper we adopt the garnet-orthopyroxene thermobarometer corrected by Pattison et al. (2003) to estimate peak and pre-peak P-T conditions of the studied UHT metapelitic granulite, and the average P-T method of Powell and Holland (1994) is used to estimate the texturally equilibrated M3 mineral assemblage. The P-T estimate results are listed in Table 2.

Low-Al orthopyroxene inclusion in garnet and the garnet in contact with the inclusion can be used to estimate P-T conditions of pre-peak metamorphic stage (M1), and the calculated results

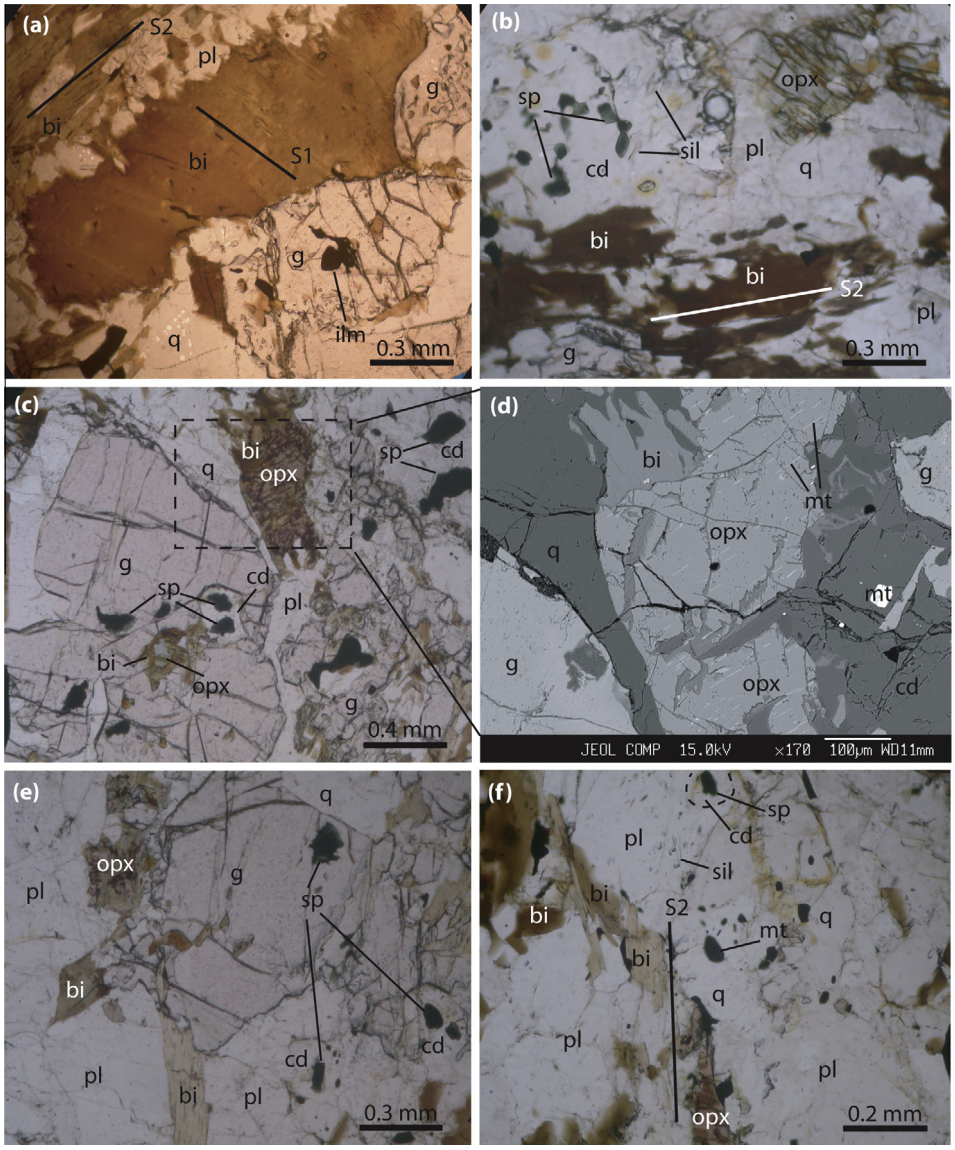

Fig. 3. Textural relations of the UHT metapelitic granulite in the Chinese Altai, in which (a–c), (e) and (f) are microphotographs in plane-polarized light, but (d) is backscattered image. (a) Two phases of gneissic foliation S1 and S2 defined by different orientation of biotite flakes, and garnet contains biotite and ilmenite inclusions; (b) cordierite contains spinel and sillimanite inclusions; (c) garnet porphyroblast contains orthopyroxene and spinel inclusions, with retrograde biotite and cordierite around them, respectively; (d) Al-rich orthopyroxene contains oriented acicular magnetite; (e) equilibrated peak assemblage g–bi–opx–pl–cd–q; and (f) M2 mineral assemblage opx–bi–sil–mt–pl–q showing marked preferred orientation. Mineral abbreviations: g, garnet; opx, orthopyroxene; sil, sillimanite; cd, cordierite; sp, spinel; bi, biotite; pl, plagioclase; ilm, ilmenite; mt, magnetite; and q, quartz.

indicate that P-T conditions of ~7.0 kbar/~890 °C. Garnet cores are inferred to have equilibrated with high-Al orthopyroxene, and thus their compositions give estimates of the UHT formation conditions at the peak stage (M2), ~8.0 kbar/~970 °C. Because post-peak orthopyroxene–biotite–sillimanite-bearing HT mineral assemblage (M3) does not contain garnet, and the garnet–orthopyroxene thermobarometer cannot be used to estimate its P-T conditions. The average P-T calculation method of Powell and Holland (1994) can be utilised to estimate post-peak HT formation conditions associated with this assemblage (M3), and indicate P-T conditions of ~9.0 kbar/~870 °C (Table 2).

As the studied UHT metapelitic mineral assemblages contain magnetite and ilmenite, the petrogenetic grid for the metapelites in the KFMASHTO model system (Fig. 5) (White et al., 2002) can be used to better constrain the P-T evolution path of the UHT metapelitic granulite. For instance, the above P-T conditions of three different metamorphic stages define an anticlockwise P-T path of initial prograde heating and increase in pressure followed by a post-peak near isobaric cooling (Fig. 5). P-T conditions of ~7.0 kbar/~890 °C for pre-peak spinel–orthopyroxene-bearing or spinel–sillimanite-bearing inclusion assemblage (M1) are consistent with the medium–low-pressure HT stability field that contains spinel-bearing assemblages in the petrogenetic grid. Furthermore, P-T conditions of ~8.0 kbar/~970 °C for peak UHT metamorphic stage (M2) are compatible with the high-Al feature (Al_2O_3 > 8.0 wt.%) in peak orthopyroxene indicating a UHT metamorphic condition (>900 °C). P-T conditions of ~9.0 kbar/~870 °C for post-peak orthopyroxene–sillimanite–biotite-bearing HT mineral assemblage (M3) are consistent with the medium-pressure HT stability field in the petrogenetic grid (Fig. 5). This suggests that if biotite and orthopyroxene–sillimanite–quartz are a paragenetic association, they cannot be used to indicate a UHT metamorphic condition.

The above anticlockwise P-T path in the KFMASHTO system explains the development of mineral assemblages and textural relations in the UHT metapelitic granulite. For example, several

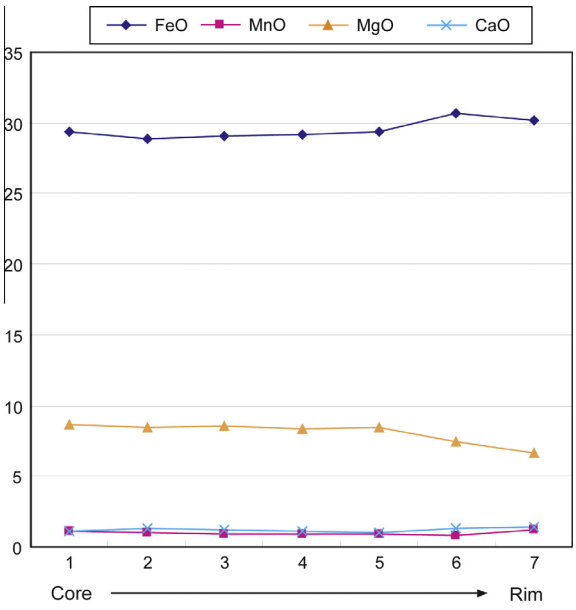

Fig. 4. Composition variation diagram of a garnet porphyroblast from core to rim.

reactions that the P-T path crossed are mainly K-feldspar-consuming reactions such as: (1) opx + cd + ksp + ilm + liq = g + bi + mt, and (2) g + cd + ksp + ilm = opx + sil + bi + mt (Fig. 5). As reaction (2) progressed, K-feldspars broke down and disappeared, and hence is not preserved in the UHT metapelitic assemblages. Oriented magnetite needles in peak Al-rich orthopyroxenes very likely formed through exsolution during post-peak cooling, whereas the reaction (2) resulted in the formation of a stable M3 mineral assemblage of orthopyroxene–sillimanite–biotite–magnetite–plagioclase–quartz.

5. P-T pseudosection calculation

P-T pseudosection calculation for particular bulk compositions in a model system has been widely used to infer metamorphic process and the P-T path that produced mineral assemblages and reaction textures in the metapelites, with the help of the Thermocalc program (Powell et al., 1998; White et al., 2007). In this study, the mineral assemblages in the UHT metapelitic granulite will be quantitatively modelled in the NCKFMASHTO system in order to constrain its metamorphic P-T history. Following the method of White et al. (2007) for the metapelites with quartz and ilmenite in excess, a P-T pseudosection is then calculated for the mineral assemblages in the UHT metapelitic granulite (LT10F) (Fig. 6).

The particular bulk composition for the UHT metapelitic granulite is estimated at first as H_2O:SiO_2:Al_2O_3:CaO:MgO:FeO:K_2O:Na_2O:TiO_2:O = 0.30:55.82:13.13:1.58:11.91:13.54:1.40:1.23:0.72:0.68, through bulk rock chemical analysis. The H_2O is set such that the rock was just water saturated at the wet solidus (Tong and Wilson, 2006). The calculated P-T pseudosection consists of various uni- and multi-variant equilibrated mineral assemblages, and shows that peak M2 garnet–orthopyroxene–cordierite–K-feldspar-bearing mineral assemblage formed under UHT conditions of 7–8 kbar and 900–980 °C, which are further compatible with the peak M2 P-T conditions of ~8.0 kbar/~970 °C estimated from the garnet–orthopyroxene thermobarometer (Fig. 6). Pre-peak spinel–orthopyroxene-bearing M1 inclusion assemblage is not well modelled, but the orthopyroxene-bearing assemblage shows a wide P-T range of 5–7 kbar and 850–950 °C, which is roughly consistent with the M1 P-T estimates of ~7.0 kbar/~890 °C from thermobarometer. However, the P-T pseudosection shows that post-peak orthopyroxene–biotite–sillimanite–magnetite-bearing M3 assemblage is stable under conditions of 6–8 kbar and 700–870 °C, implying that the M3 P-T estimates from thermobarometer may not be overestimated (Fig. 6). This is probably because that orthopyroxene–biotite–sillimanite–magnetite-bearing M3 assemblage contains K-feldspar in the NCKFMASHTO system makes the actual P-T stability field of the K-feldspar-absent M3 assemblage lower. Furthermore, the pseudosection also indicates that M3 assemblage might contain late garnet. In summary, the P-T pseudosection calculated for the UHT metapelitic granulite in this study apparently indicates a post-peak near-isobaric cooling anticlockwise P-T path (Fig. 6). However, the absence of K-feldspar in the rock suggests that the P-T path derived from the studied sample may be interpreted better by the P-T petrogenetic grid in the KFMASHTO system (Fig. 5) than by the P-T pseudosection in the NCKFMASHTO system (Fig. 6).

6. SHRIMP zircon U–Pb ages

Conventional magnetic and heavy liquid techniques followed by hand-picking under a binocular microscope were used for separation of zircon from the metapelitic granulite. The morphology and internal structure of the zircons were documented with transmitted and reflected light microphotographs and cathodoluminescene (CL) images. The zircon grains were analysed using the SHRIMP ion microprobe at the Beijing SHRIMP Centre, Chinese Academy of Geological Sciences, using the standard operating conditions outlined by Williams (1998). Th–U–Pb ratios were determined relative to the TEMORA standard zircon, and the absolute abundances of U and Th relative to the SL13 standard zircon. Pb_c and Pb^* represent the common and radiogenic portions, respectively, and common Pb was corrected using measured ^{204}Pb.

Table 2
P-T estimate results for three-stage mineral assemblages in the UHT metapelitic granulite. The corrected garnet–orthopyroxene thermobarometers of Pattison et al. (2003) are applied for estimating M1 and M2 P-T conditions, while the average P-T method of Powell and Holland (1994) is used for M3 P-T estimates. The fit value for M3 P-T estimates is less than 1.61, suggesting that the average P-T calculation falls within 95% confidence level.

Model 1	Model 2	Model 3	Model 4	Average	
M1:					
T = 887 ± 44 °C	T = 891 ± 45 °C	T = 891 ± 45 °C	T = 881 ± 44 °C	T = 888 ± 44 °C	
P = 7.0 ± 0.4 kbar	P = 7.1 ± 0.4 kbar	P = 7.1 ± 0.4 kbar	P = 7.0 ± 0.4 kbar	P = 7.1 ± 0.4 kbar	
M2:					
T = 984 ± 49 °C	T = 962 ± 48 °C	T = 966 ± 48 °C	T = 959 ± 48 °C	T = 968 ± 48 °C	
P = 8.1 ± 0.4 kbar	P = 7.9 ± 0.4 kbar	P = 7.9 ± 0.4 kbar	P = 7.9 ± 0.4 kbar	P = 8.0 ± 0.4 kbar	
M3:					
avP (kbar)	sd	avT (°C)	sd	cor	fit
9.0	1.1	872	108	0.701	1.41

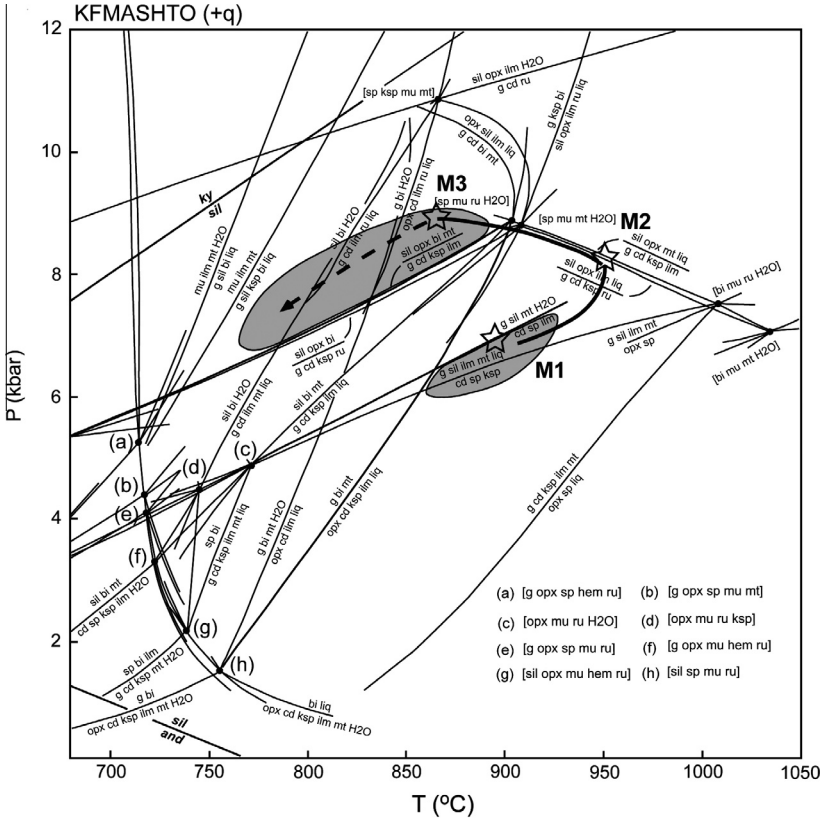

Fig. 5. P-T projection in the KFMASHTO system for metapelites, showing the P-T path of the UHT metapelitic granulite in the Chinese Altai orogen (after White et al., 2002). Mineral abbreviations: ksp, K-feldspar; ky, kyanite; mu, muscovite; ru, rutile; liq, melt; others are same as those in Fig. 2.

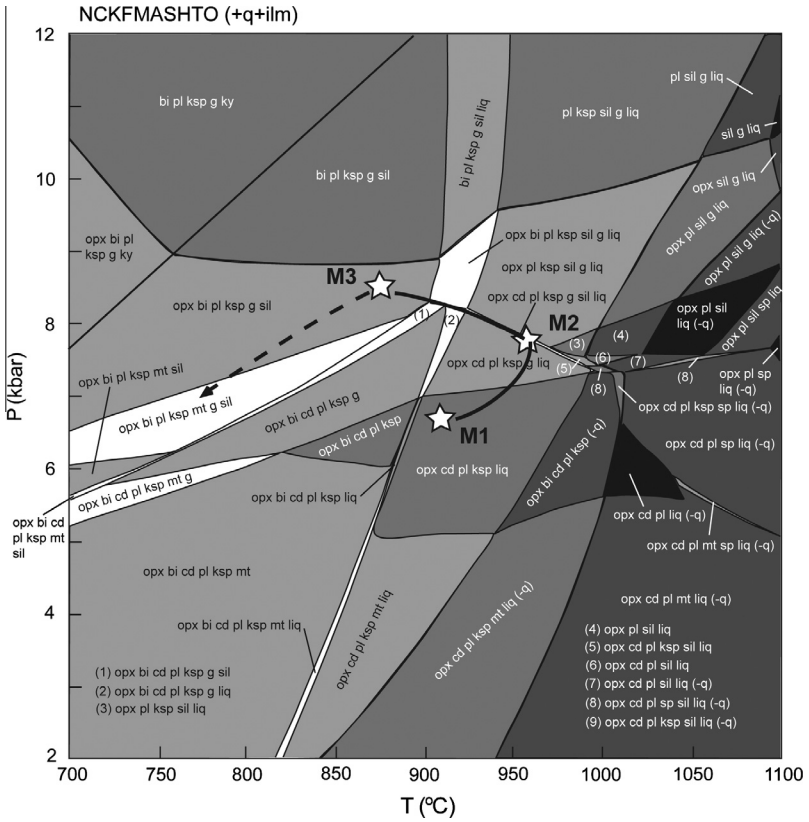

Fig. 6. P-T pseudosection calculated for the studied UHT metapelitic granulite in the model NCKFMASHTO system with quartz and ilmenite in excess.

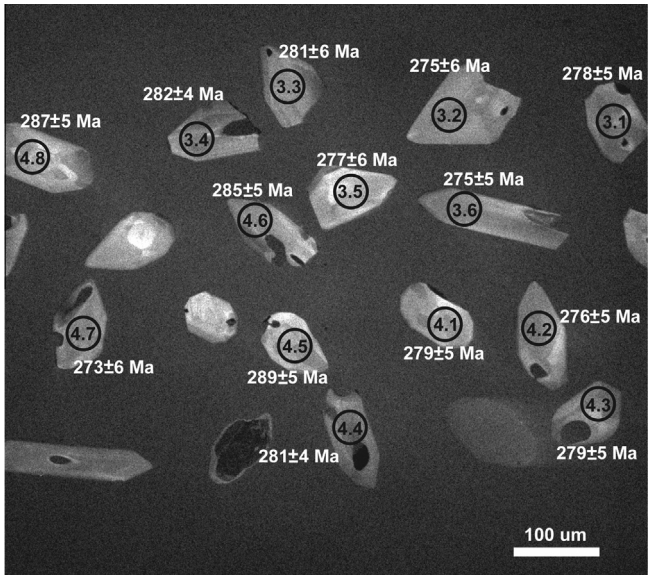

Fig. 7. The CL images for representative zircons in the UHT metapelitic granulite.

Software SQUID 1.0 and ISOPLOT (Ludwig, 1999) were used for data processing. The weighted mean ages are quoted at the 95% confidence level.

Representative CL images of zircons in the UHT metapelitic granulite from the Altai orogen are shown in Fig. 7, and SHRIMP zircon U–Pb analysis data and age results are listed in Table 3 and shown in Fig. 8. Zircons in the UHT metapelitic granulite are euhedral to semi-euhedral with length to width ratios of 2:1 to 4:1. Their images are mainly light gray in colour, and lack magmatic oscillatory or rhythmic zoning (Fig. 7).

Table 3 shows that the zircon ages are mostly distributed between 285 and 270 Ma, and their calculated $^{206}Pb/^{238}U$ age is 278 ± 2 Ma (n = 33, MSWD = 1.2), with a weighted mean age of 278 ± 2 Ma (Fig. 8). The Th/U ratios of the analysed zircons are relatively high, ranging from 0.71 and 0.90. The CL imaging is consistent with the grains forming through recrystallization during the UHT granulite metamorphism. Therefore, the U–Pb age of 278 ± 2 Ma is interpreted to reflect the time of the UHT metamorphic event in the Chinese Altai orogenic belt. This age shows a better precision than the U–Pb zircon age of 271 ± 5 Ma obtained recently by the LA-ICP-MS technique from the same UHT metapelitic granulite in the study region (Tong et al., 2013).

7. Discussion

Detailed petrographic observations, mineral compositions and P-T estimates, indicate the existence of a garnet–orthopyroxene–sillimanite–cordierite-bearing UHT metapelitic granulite near Kalasu, within the Altai orogenic belt. Peak orthopyroxene has an Al_2O_3 as high as 9.0 wt.%, suggesting that peak metamorphism reached UHT conditions (>900 °C). P-T estimates indicate peak metamorphic conditions of ~8.0 kbar/~970 °C, whereas P-T conditions of three different metamorphic stages define an anticlockwise P-T path of initial prograde up-pressure and heating and post-peak near isobaric cooling in the petrogenetic grid for the KFMASHTO model system (White et al., 2002) (Fig. 5). The anticlockwise P-T path of post-peak near isobaric cooling often reflects a tectonic process involving initial crustal compression immediately followed by extension, and this process is normally accompanied by intrusions of deep-derived magma or thinning of mantle

Table 3
SHRIMP U–Pb analysis results for zircons in the UHT metapelitic granulite.

Spot	% $^{206}Pb_c$	U	Th	Th/U	$^{207}Pb^*/^{206}Pb^*$	%	$^{207}Pb^*/^{235}U$	%	$^{206}Pb^*/^{238}U$	%	$^{207}Pb/^{206}Pb$ (Ma)	1s err	$^{208}Pb/^{232}Th$ (Ma)	1s err	$^{206}Pb/^{238}U$ (Ma)	1s err
LT10F-1.1	0.16	195	142	0.75	.0568	6.0	0.345	6.3	.0441	2.1	485.2	132	285.3	12	278.1	5.7
LT10F-1.2	0.29	152	114	0.78	.0566	6.0	0.342	6.2	.0438	1.7	476.0	132	287.5	12	276.5	4.6
LT10F-1.3	1.53	195	147	0.78	.0443	20.0	0.261	20.1	.0427	1.9	−91.7	490	255.0	26	269.7	5.0
LT10F-1.4	2.01	162	122	0.78	.0432	18.7	0.262	18.8	.0439	2.0	−158.0	464	249.7	24	277.2	5.4
LT10F-2.2	1.67	182	127	0.72	.0423	22.8	0.252	22.9	.0432	2.0	−206.8	572	263.2	30	272.4	5.4
LT10F-2.3	0.15	279	237	0.88	.0544	3.9	0.326	4.2	.0434	1.5	388.1	87	279.3	8	273.9	4.1
LT10F-1.5	1.56	156	125	0.83	.0508	14.2	0.308	14.3	.0440	1.9	231.9	327	273.3	21	277.4	5.1
LT10F-1.6	1.83	247	196	0.82	.0417	12.4	0.248	12.5	.0431	1.7	−243.4	312	239.3	15	271.9	4.5
LT10F-1.7	2.34	212	162	0.79	.0431	13.1	0.258	13.2	.0435	1.9	−161.4	325	238.1	18	274.4	5.2
LT10F-3.1	1.85	165	143	0.90	.0462	11.7	0.281	11.9	.0441	1.8	7.3	283	257.8	15	278.5	4.9
LT10F-3.2	2.45	168	118	0.73	.0423	28.3	0.254	28.3	.0436	2.1	−210.2	710	250.9	37	275.3	5.8
LT10F-3.3	0.53	202	147	0.75	.0524	10.9	0.322	11.0	.0446	1.9	305.0	248	288.9	19	281.1	5.3
LT10F-3.4	0.43	221	176	0.82	.0525	7.0	0.324	7.2	.0447	1.6	306.6	159	277.0	12	282.0	4.4
LT10F-3.5	1.76	127	88	0.72	.0512	13.2	0.310	13.4	.0438	2.4	251.9	304	269.8	20	276.6	6.5
LT10F-3.6	2.69	195	137	0.73	.0497	15.8	0.299	15.9	.0436	1.8	180.4	368	269.2	25	275.1	4.9
LT10F-4.1	1.69	144	109	0.78	.0532	10.6	0.324	10.8	.0442	1.8	337.7	241	272.0	18	278.7	4.9
LT10F-4.2	1.78	164	118	0.74	.0503	12.7	0.304	12.8	.0437	1.8	211.2	294	248.3	20	275.9	4.8
LT10F-4.3	2.49	133	102	0.79	.0489	15.5	0.298	15.6	.0442	1.9	145.0	363	260.1	23	278.6	5.2
LT10F-4.4	1.63	246	178	0.75	.0444	12.4	0.272	12.5	.0445	1.6	−89.7	305	255.8	16	280.6	4.4
LT10F-4.5	1.40	132	101	0.79	.0514	11.1	0.325	11.3	.0459	1.8	259.9	256	280.0	18	289.1	5.0
LT10F-4.6	0.96	213	154	0.75	.0514	9.6	0.320	9.8	.0452	1.6	258.0	222	283.3	16	284.9	4.6
LT10F-4.7	2.59	145	107	0.77	.0405	27.7	0.242	27.8	.0432	2.1	−316.2	711	254.7	33	272.7	5.7
LT10F-4.8	1.58	143	116	0.84	.0489	11.0	0.307	11.2	.0455	1.7	145.2	259	288.4	14	286.9	4.9
LT10F-4.9	1.48	209	155	0.77	.0447	10.4	0.274	10.6	.0445	1.6	−71.9	255	259.7	15	280.6	4.5
LT10F-5.1	0.94	146	122	0.86	.0514	9.3	0.310	9.5	.0438	1.8	257.3	214	270.2	13	276.1	4.8
LT10F-5.2	1.66	209	173	0.85	.0541	8.7	0.338	8.9	.0453	1.7	376.3	196	267.9	13	285.6	4.7
LT10F-5.3	3.50	118	81	0.71	.0359	29.1	0.221	29.2	.0447	2.1	−636.7	797	236.7	33	282.0	5.7
LT10F-5.4	1.00	111	77	0.72	.0582	7.5	0.354	7.7	.0441	1.8	536.8	163	305.1	13	278.4	4.8
LT10F-5.5	1.67	113	78	0.72	.0501	12.5	0.307	12.7	.0445	1.9	200.4	291	276.4	22	280.6	5.1
LT10F-5.6	3.65	134	97	0.75	.0342	27.8	0.200	27.9	.0424	2.5	−775.5	784	217.6	29	267.8	6.5
LT10F-6.1	4.85	95	68	0.74	.0306	34.8	0.173	34.9	.0411	2.2	−1101.3	1056	206.8	32	259.4	5.5
LT10F-6.2	0.85	131	90	0.71	.0574	5.1	0.355	5.4	.0448	1.7	508.2	113	281.4	11	282.8	4.7
LT10F-6.3	2.02	176	124	0.73	.0423	26.3	0.254	26.4	.0436	2.0	−208.2	661	240.6	33	274.9	5.5

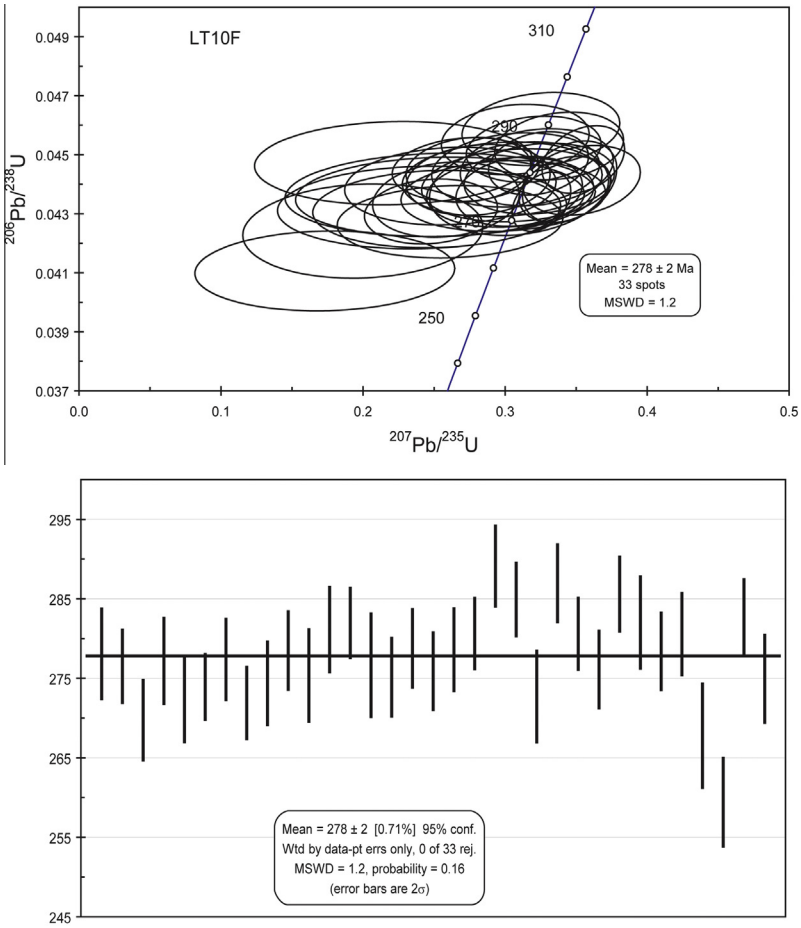

Fig. 8. U–Pb concordant age diagram for zircons in the UHT metapelitic granulite.

lithosphere, which may provide an important heat source resulting in rapid heating of thickening crust (Sandiford and Powell, 1991). Therefore, the anticlockwise P-T path of post-peak near isobaric cooling obtained in this study suggests that the Altai UHT metapelitic granulite might have formed in a tectonic setting involving intrusions of deep-derived magma and accompanied by extensional heating of the lower crust. This is consistent with the conclusion derived by Wang et al. (2009), namely the medium–low-pressure HT metapelitic granulite formed in an extensional tectonic setting of high heat flow.

The above results contrast with the inference from the UHT (>900 °C) metapelitic granulite reported by Li et al. (2010) from Wuqiagou in Fuyun county (Fig. 1). They considered that the UHT metapelitic granulite had a clockwise P-T path of post-peak decompression that they considered to be associated with oceanic crustal subduction and plate collision. Since the mineral assemblages and textural relations in the UHT metapelitic granulites from the two areas are very similar, we think that the UHT metapelitic granulite at Wuqiagou might have actually experienced an anticlockwise P-T history of post-peak near isobaric cooling similar to that of this study. Furthermore, their so-called "clockwise P-T path" has recently been changed to anticlockwise path (pers. comm. with Li). Li et al. (2010) also undertook zircon dating for the UHT metapelitic granulite at Wuqiagou and reported many grains gave ~500 Ma ages, which they suggested could be the age of either the UHT metamorphic event or of an inherited source. Subsequently, Li et al. (2012) reported a Permian zircon age (~277 Ma) in these rocks, which is identical within error to that in the present study, supporting that the Altai UHT metamorphic event occurred in the Permian. The timing of the UHT granulite facies metamorphic event is also compatible with the Permian metamorphic ages (270–280 Ma) of other medium–low-pressure HT granulites and gneisses in this orogenic belt (Table 4) (Chen et al., 2006b; Wang et al., 2009; Hu et al., 2006; Zheng et al., 2007), suggesting a widespread Permian pulse of UHT and HT granulite facies metamorphism in the Altai orogenic belt. As the UHT metapelitic granulite occurs as tectonic lenses within the medium–low pressure high-temperature metapelitic granulites, this implies that the UHT metapelitic granulite might have been emplaced into the medium–low pressure high-temperature metapelitic granulites through D2 tectonism.

The Permian age of the Altai UHT metamorphic event is equivalent with the Permian Tarim mantle plume activity in Xinjiang (~275 Ma) (Zhang et al., 2010), and is also well compatible with the timing of the extensive Permian (280–260 Ma) mantle-derived mafic to granitic magmatism that formed in a post-orogenic or anorogenic extensional setting in the Altai region (Table 4) (Han et al., 2004; Chen and Han, 2006; Tong et al., 2006b; Briggs et al., 2007; Zhang et al., 2012). Thus, the UHT metamorphism might have been caused by deeply derived magma that heated the lower crust during extension and mantle plume activity in the Permian. For instance, the post-orogenic or anorogenic Lamazhao granite and Fuyun granitic dykes were respectively intruded at 276 ± 9 Ma and 275 ± 2 Ma (Wang et al., 2005; Tong et al., 2006a), and they were derived from underplating of post-orogenic mantle-derived mafic magma (Tong et al., 2006b), whilst the Kalatongke mafic intrusive complex (287 ± 5 Ma) in Fuyun county was also considered to have formed during an underplating of

Table 4
Summary of the Permian isotopic ages reported from the Chinese Altai orogen.

Locations	Rocks	Methods	Ages (Ma)	References
Qinghe	Gneiss	SHRIMP	281 ± 3	Hu et al. (2006)
Fuyun	Mafic granulite	SHRIMP	279 ± 6	Chen et al. (2006b)
Fuyun	Gneiss	In situ Th–Pb	278 ± 9, 275 ± 8	Briggs et al. (2007)
Altai–Qinghe	Gneiss	CHIME	261–268	Zheng et al. (2007)
Kalasu	Pelitic granulite	SHRIMP	293 ± 2	Wang et al. (2009)
Fuyun	Pelitic granulite	LA-ICP-MS	269–292	Li et al. (2012)
Qinghe	Gabrro	SHRIMP	272 ± 2	Zhang et al. (2010)
Fuyun–Qinghe	Granite	SHRIMP	283 ± 4	Zhang et al. (2012)
Kalatongke	Mafic Complex	SHRIMP	287 ± 5	Han et al. (2004)
Huangshandong	Mafic Intrusion	SHRIMP	269 ± 2	Zhou et al. (2004)
E Junger	Granitoid	Rb–Sr	294 ± 4	Chen and Jahn (2004)
Lamazhao	Granite	SHRIMP	276 ± 9	Wang et al. (2005)
Fuyun	Granite	TIMS	281 ± 5, 275 ± 2	Tong et al. (2006a)
Qinghe	Granite	SHRIMP	283 ± 4	Zhou et al. (2007)
Fuyun	Mafic intrusion	SHRIMP	257, 280	Chen and Han (2006)

mantle-derived magma in a post-orogenic extensional setting (Han et al., 2004). Moreover, mantle-derived Permian mafic intrusions also occur in the study area (Fig. 2). All these support the existence of a Permian mantle plume activity (~275 Ma) in the Altai region (Pirajno et al., 2008; Zhang et al., 2012). Therefore, the Altai UHT metamorphic event might be closely associated with underplating of mantle-derived magma and extensional heating of lower crust caused by the Permian Tarim mantle plume activity. In addition, the anticlockwise P-T paths recorded from the granulites in the North China craton have been attributed to mantle plume activity (Zhao et al., 1999). Thus, this is not only consistent with the tectonic setting reflected by the anticlockwise P-T path, but also compatible with the development of several granitic-gneissic thermal dome structures in the Altai region (Zhuang, 1994).

Since the early amphibolite facies metamorphism in the Altai orogenic belt occurred in the Devonian (Wei et al., 2007), this phase of metamorphism was ascribed to either an arc-continent collision (Windley et al., 2002; Wang et al., 2006) or a ridge-subduction and slab-window (Windley et al., 2007; Sun et al., 2009; Jiang et al., 2010), which formed the framework of this orogenic belt. In this case, the Permian UHT metamorphic event is also consistent with the time of the large Erqis shear zone (Briggs et al., 2007), along which the voluminous A-type granites and anorogenic mafic intrusions emplaced at the same time (Zhang et al., 2012). This suggests that the movement of the large Erqis shear zone was likely coupling with the mantle plume activity, and was associated with intraplate reworking. Therefore, this Permian UHT metamorphism in the Chinese Altai orogen should reflect an overprinting metamorphic event caused by the Permian Tarim mantle plume activity, rather than a late Palaeozoic oceanic crustal subduction and plate collision that resulted in the HT or UHT granulite metamorphism (Chen et al., 2006a; Li et al., 2012).

8. Conclusions

(1) Petrography, mineral compositions and metamorphic P-T estimates results for a garnet–orthopyroxene–sillimanite–cordierite-bearing UHT metapelitic granulite from the Altai orogenic belt near Kalasu, southeast of Aletai city, show Al_2O_3 as high as 9.0 wt.% in orthopyroxene and peak P-T conditions of ~8.0 kbar and ~970 °C, and a post-peak near isobaric cooling anticlockwise P-T path.
(2) The SHRIMP zircon U–Pb age dating of a UHT metapelitic granulite yielded a concordant age of 278 ± 2 Ma, indicating that UHT metamorphism in the Chinese Altai occurred in the Permian.
(3) The UHT metamorphic event occurred synchronously with the Permian (~280 Ma) post-orogenic mantle-derived mafic intrusions related to the Permian (~275 Ma) Tarim mantle plume activity, suggesting that the Permian UHT metamorphism in the Chinese Altai might be closely associated with mantle underplating, heating and post-orogenic extension.

Acknowledgements

This study has been financially supported by the Chinese National Key Basic Development Project "973" (2011CB808901). The Electron Microprobe analysis mineral composition was finished with help of Ms L.L. Chen at State Key Lab of Isotope Geochemistry, Guangzhou Institute of Geochemistry. Zircon U–Pb age analyses via SHRIMP II ion microprobe were completed with help of Dr. J.H. Liu at the Beijing SHRIMP Centre, Chinese Academy of Geological Sciences. We appreciate the constructive comments and suggestions of journal Editor Prof. J.G. Liou, C.M. Wu and an anonymous reviewer that significantly improved the manuscript. This is contribution No. IS-1864 from GIG-CAS.

References

Briggs, S.M., Yin, A., Manning, C.E., Chen, Z.L., Wang, X.F., Grove, M., 2007. Late paleozoic tectonic evolution history of the Ertix fault in the Chinese Altai and its implications for the development of the central asian orogenic system. GAS Bull. 119, 944–960.
Brown, M., 2007. Metamorphic conditions in orogenic belts: a record of secular change. Int. Geol. Rev. 49, 193–234.
Cawood, P.A., Kröner, A., Collins, W.J., Kusky, T.M., Mooney, W.D., Windley, B.F., 2009. Accretionary Orogens through Earth history. In: Cawood, P.A., Kröner, A. (Eds.), Earth Accretionary Systems in Space and Time, vol. 318. Geological Society Special Publication, pp. 1–36.
Chen, B., Jahn, B.-M., 2004. Genesis of post-collisional granitoids and basement nature of the Junggar Terrane, NW China: Nd–Sr isotope and trace element evidence. J. Asian Earth Sci. 23, 691–703.
Chen, H., Li, Z., Yang, S., Dong, C., Xiao, W., Tainosho, Y., 2006a. Mineralogical and geochemical study of a newly discovered mafic granulite, northwest China: implications for tectonic evolution of the Altay orogenic belt. Island Arc 15, 210–222.
Chen, H., Yang, S., Li, Z., Yu, X., Xiao, W., Yuan, C., Li, J., 2006b. Zircon SHRIMP U–Pb chronology of the Fuyun basic granulite and its tectonic significance in the Altaid orogenic belt. Acta Petrol. Sin. 22, 1351–1358 (in Chinese with English abstract).
Chen, L., Han, B., 2006. Geochronology, geochemistry and Sr–Nd–Pb isotopic composition of mafic intrusive rocks in Wuqiagou area, north Xinjiang: constraints for mantle sources and deep processes. Acta Petrol. Sin. 22, 1201–1214 (in Chinese with English abstract).
Han, B., Ji, J., Song, B., Chen, L., Li, Z., 2004. SHIMP zircon U–Pb age of Kalatongke No. 1 and Huangshandong Cu–Ni-bearing mafic-ultramafic complexes, North Xinjiang, and geological implications. Chin. Sci. Bull. 49, 2424–2429.
Harley, S.L., 2004. Extending our understanding of ultrahigh temperature crustal metamorphism. J. Mineral. Petrol. Sci. 99, 140–158.
Harley, S.L., 2008. Refining the P-T records of UHT crustal metamorphism. J. Metamorph. Geol. 26, 125–154.
Harley, S.L., Motoyoshi, Y., 2000. Al zoning in orthopyroxene in a sapphirine quartzite: evidence for >1120 °C UHT metamorphism in the Napier Complex,

Antarctica, and implications for the entropy of sapphirine. Contrib. Miner. Petrol. 138, 293–307.
He, G., Han, B., Yue, Y., Wang, J., 1990. Tectonic division and crustal evolution of Altay orogenic belt in China. Geosci. Xinjiang 2, 9–20 (in Chinese with English abstract).
Hu, A., Zhang, G., Zhang, Q., Li, T., Zhang, J., 2002. A review on ages of Precambrian metamorphic rocks from Altai orogen in Xinjiang, NW China. Chin. J. Geol. 37, 129–142 (in Chinese with English abstract).
Hu, A., Wei, G., Deng, W., Chen, L., 2006. SHRIMP zircon U–Pb dating and its significance for gneisses from the southwest area to Qinghe county in Xinjiang, NW China. Acta Petrol. Sin. 22, 1–20 (in Chinese with English abstract).
Jahn, B.-M., 2004. The central asian orogenic belt and growth of the continental crust in the phanerozoic. In: Malpas, J., Fletcher, C.J.N., Ali, J.R., Aitchison, J.C. (Eds.), Aspects of the Tectonic Evolution of China, 226. Geological Society Special Publications, pp. 73–100.
Jahn, B.-M., Windley, B., Natal'in, B., Dobretsov, N., 2004. Phanerozoic continental growth in central Asian. J. Asian Earth Sci. 23, 599–603.
Jiang, Y., Sun, M., Zhao, G., Yuan, C., Xiao, W., Xia, X., Long, X., Wu, F., 2010. The ~390 Ma high-*T* metamorphic event in the Chinese Altai: a consequence of ridge-subduction? Am. J. Sci. 310, 1421–1452.
Laurent-Charvet, S., Charvet, J., Monie, P., Shu, L., 2003. Late paleozoic strike-slip shear zones in eastern central Asia (NW China): new structural and geochronological data. Tectonics 22, 1009. http://dx.doi.org/10.1029/2001TC901047.
Li, Z., Chen, H., Yang, S., Xiao, W., Tainosho, Y., 2004. Discovery of the basic granulite from the Altai area: evidence from mineralogy. Acta Petrol. Sin. 20, 1445–1455 (in Chinese with English abstract).
Li, Z., Li, Y., Chen, H., Santosh, M., Xiao, W., Wang, H., 2010. SHRIMP U–Pb zircon chronology of ultrahigh-temperature spinel–orthopyroxene–garnet granulite from south Altay orogenic belt, Northwestern China. Island Arc 19, 506–516.
Li, Z., Li Y., Wang, H., Chen, H., Yang, X., 2012. Late palaeozoic ultrahigh temperature metamorphism of the Altai and its evolution. In: 2012 National Symposium on Petrology and Geodynamics (abst), p. 319. (in Chinese).
Long, X., Sun, M., Yuan, C., Xiao, W., Lin, S., Wu, F., Xia, X., Cai, K., 2007. Detrital zircon age and Hf isotopic studies for metasdimentary rocks from the Chinese Altai: implications for the early paleozoic tectonic evolution of the central Asian orogenic belt. Tectonics 26, TC5015. http://dx.doi.org/10.1029/2007TC002128.
Ludwig, K.R., 1999. Using Isoplot/EX, version 2. A Geological Toolkit for Microsoft Excel. Berkeley Geochronological Center, Special Publication 1a, p. 47.
Pattison, D.M., Chacko, T., Farquhar, J., McFarlane, C.R.M., 2003. Temperatures of granulite-facies metamorphism: constraints from experimental phase equilibria and thermobarometry corrected for retrograde exchange. J. Petrol. 44, 867–900.
Pirajno, F., Mao, J., Zhang, Z., Zhang, Z., Chai, F., 2008. The association of mafic-ultramafic intrusions and A-type magmatism in the Tian Shan and Altay orogens, NW China: implications for geodynamic evolution and potential for the discovery of new ore deposits. J. Asian Earth Sci. 32, 165–183.
Powell, R., Holland, T., 1994. Optimal geothermometr and geobarometry. Am. Mineral. 79, 120–133.
Powell, R., Holland, T., Worley, B., 1998. Calculating phase diagrams involving solid solutions via non-linear equations, with examples using THERMOCALC. J. Metamorph. Geol. 16, 577–588.
Raith, M., Karmakar, S., Brown, M., 1997. Ultrahigh-temperature metamorphism and multi-stage decompressional evolution of sapphirine–granulites from Palni hill ranges, southern India. J. Metamorph. Geol. 15, 379–399.
Sandiford, M., Powell, R., 1991. Some remarks on high-temperature-low-pressure metamorphism in convergent orogens. J. Metamorph. Geol. 9, 333–340.
Santosh, M., Tsunogae, T., Li, J., Liu, S., 2007. Discovery of sapphirine-bearing Mg–Al granulites in the north China Craton: implications for palaeoproterozoic ultrahigh-temperature metamorphism. Gondwana Res. 11, 263–285.
Sengör, A.M.C., Natal'in, B.A., Burtman, V.S., 1993. Evolution of the Altaid tectonic collage and Palaeozoic crustal growth in Eurasia. Nature 54, 117–137.
Sun, M., Yuan, C., Xiao, W., Long, X., Xia, X., Zhao, G., Lin, S., Wu, F., Kroner, A., 2008. Zircon U–Pb and Hf isotopic study of gneissic rocks from the Chinese Altai: progressive accretionary history in the early to middle paleozoic. Chem. Geol. 247, 352–383.
Sun, M., Long, X., Cai, K., Jiang, Y., Wang, B., Yuan, C., Zhao, G., Xiao, W., Wu, F., 2009. Early palaeozoic ridge subduction in the Chinese Altai: insight from the abrupt change in zircon Hf isotopic compositions. Sci. China (Ser. D) 52, 1345–1348.
Tong, L., Wilson, C.J.L., 2006. Tectonothermal evolution of the ultrahigh temperature metapelites in the Rauer Group, east Antarctica. Precambr. Res. 149, 1–20.
Tong, Y., Hong, D., Wang, T., Wang, S., Han, B., 2006a. TIMS U–Pb zircon ages of Fuyun post-orogenic linear granite plutons on the southern margin of Altay orogenic belt and their implications. Acta Petrol. Mineral. 25, 85–89 (in Chinese with English abstract).
Tong, Y., Wang, T., Hong, D., Han, B., 2006b. Pb isotopic compositions of granitoids from the Altay Orogen (China): evidence for mantle-derived origin and continental growth. Acta Geol. Sinica 40, 517–528 (in Chinese with English abstract).
Tong, L., Chen, Y., Xu, Y., Zhou, X., Liu, Z., 2013. Zircon U–Pb ages of the ultrahigh-temperature metapelitic granulite from the Altai orogeny, NW China, and geological implications. Acta Petrol. Sin. 29, 3435–3445 (in Chinese with English abstract).
Wang, T., Hong, D., Tong, Y., Han, B., Shi, Y., 2005. Zircon U–Pb SHRIMP age and origin of post-orogenic Lamazhao granite pluton from Altai orogen: its implications for vertical continental growth. Acta Petrol. Sin. 21, 640–650 (in Chinese with English abstract).
Wang, T., Hong, D., Jahn, B.-M., Tong, Y., Wang, Y., Han, B., Wang, X., 2006. Timing, petrogenesis, and setting of paleozoic synorogenic intrusions from the Altai Mountains, Northwest China: implications for the tectonic evolution of an accretionary orogen. J. Geol. 114, 735–751.
Wang, T., Jahn, B.-M., Kovach, V.P., Tong, Y., Hong, D., Han, B., 2009a. Nd–Sr isotopic mapping of the Chinese Altai and implications for continental growth in the central Asian orogenic belt. Lithos 110, 359–372.
Wang, W., Wei, C., Wang, T., Lu, Y., Chu, H., 2009b. Determination of pelitic granulites in the Chinese Altai orgenic belt and geological implications. Chin. Sci. Bull. 54, 918–923 (in Chinese).
Wei, C., Clarke, G., Tian, W., Qiu, L., 2007. Transition of metamorphic series from the kyanite- to andalusite-types in the Altai orogen, Xinjiang, China: evidence from petrography and calculated KMnFMASH and KFMASH phase relations. Lithos 96, 353–374.
White, R.W., Powell, R., Clarke, G.L., 2002. The interpretation of reaction textures in Fe-rich metapelitic granulites of the Musgrave Block, central Australia: constraints from mineral equilibria calculations in the system K_2O–FeO–MgO–Al_2O_3–SiO_2–H_2O–TiO_2–Fe_2O_3. J. Metamorph. Geol. 20, 41–55.
White, R.W., Powell, R., Holland, T.J.B., 2007. Progress related to calculation of partial melting equilibria for metapelites. J. Metamorph. Geol. 25, 511–527.
Williams, I.S., 1998. U–Th–Pb geochronology by ion microprobe. Rev. Econ. Geol. 7, 1–35.
Windley, B.F., Kroner, A., Guo, J., Qu, G., Li, J., Zhang, C., 2002. Neoproterozoic to Paleozoic geology of the Altai orogen, NW China: new zircon age data and tectonic evolution. J. Geol. 110, 719–737.
Windley, B.F., Alexeiev, D., Xiao, W., Kroner, A., Badarch, G., 2007. Tectonic models for accretion of the Central Asian Orogenic belt. J. Geol. Soc., London 164, 31–47.
Xiao, W., Windley, B.F., Badarch, G., Sun, S., Li, J., Qin, K., Wang, Z., 2004. Palaeozoic accretion and convergent tectonics of the southern Altaids: implications for the growth of Central Asia. J. Geol. Soc., London 161, 339–342.
Xiao, W., Han, C., Yuan, C., Chen, H., Sun, M., Lin, S., Li, Z., Mao, Q., Zhang, J., Sun, S., Li, J., 2006. Unique carboniferous-permian tectonic-metallogenic framework of northern Xinjiang (NW China): constraints for the tectonics of the southern palaoasian domain. Acta Petrol. Sin. 22, 1062–1076 (in Chinese with English abstract).
Xiao, W., Han, C., Yuan, C., Sun, M., Lin, S., Chen, H., Li, Z., Li, J., Sun, S., 2008. Middle cambrian to permian subduction-related accretionary orogenesis of Northern Xinjiang, NW China: implications for the tectonic evolution of central Asia. J. Asian Earth Sci. 32, 102–117.
Xiao, W., Huang, B., Han, C., Sun, S., Li, J., 2010. A review of the western part of the Altaids: a key to understanding the architecture of accretionary orogens. Gondwana Res. 18, 253–273.
Xu, X., Zheng, C., Zhao, Q., 2005. Metamorphic types and crustal evolution of Hercynian orogenic belt in Altai region, Xinjiang. J. Jilin Univ. 35, 7–11 (in Chinese with English abstract).
Yuan, C., Sun, M., Xiao, W., Li, X., Chen, H., Lin, S., Xia, X., Long, X., 2007. Accretionary orogenesis of the Chinese Altai: insights from Palaeozoic granitoids. Chem. Geol. 242, 22–39.
Zhang, C., Wei, C., Qiu, L., 2004. Evolution of metamorphism and its geologic significance in Altaids, Xinjiang. Xinjiang Geol. 22, 16–23 (in Chinese with English abstract).
Zhang, C.L., Li, Z.X., Li, X.H., Xu, Y.G., Zhou, G., Ye, H.M., 2010. A Permian large igneous province in Tarim and Central Aisian orogenic belt, NW China: results of a ca. 275 Ma mantle plume? Geol. Soc. Am. Bull. 122, 2020–2040.
Zhang, C.L., Santosh, M., Zou, H.B., Xu, Y.G., Zhou, G., Dong, Y.G., Ding, R.F., Wang, H.Y., 2012. Revisiting the "Irtish tectonic belt": implications for the Palaeozoic tectonic evolution of the Altai orogen. J. Asian Earth Sci. 52, 117–133.
Zhao, G., Wilde, S.A., Cawood, P.A., Lu, L., 1999. Thermal evolution of two textural types of mafic granulites in the North China craton: evidence for both mantle plume and collisional tectonics. Geol. Mag. 136, 223–240.
Zheng, C.Q., Kato, T., Enami, M., Xu, X.C., 2007. CHIME monazite ages of metasediments from the Altai orogen in northwestern China: Devonian and permian ages of metamorphism and their significance. Island Arc 16, 598–604.
Zhou, G., Zhang, Z.C., Luo, S.B., He, B., Wang, X., Ying, L.J., Zhao, H., Li, A.H., He, Y.K., 2007. Confirmation of high-temperature strongly peraluminous Mayin'ebo granites in the margin of Altay, Xinjiang: age, geochemistry and tectonic implications. Acta Petrol. Sin. 23, 1909–1920 (in Chinese with English abstract).
Zhou, M.F., Lesher, C.M., Yang, Z., Li, J., Sun, M., 2004. Geochemistryand petrogenesis of 270 Ma Ni–Cu-(PGE)sulfide-bearing mafic intrusions in the Huangshan district, eastern Xinjiang, northwest China: implications for the tectonic evolution of the central Asian orogenic belt. Chem. Geol. 209, 233–257.
Zhuang, Y., 1994. The PTSt evolution of metamorphism and development mechanism of the thermal structural gneiss domes in the Chinese Altaides. Acta Geol. Sin. 68, 35–47 (in Chinese with English abstract).